parallel to the incident electron waves.

By knowing the tubule diameter D and its pitch angle α with respect to the fibre axis (Fig. 3*a*), the helicity and thus the tubule structure can be determined uniquely. To describe the tubule helicity, we follow Hamada's notation[6] as illustrated in Fig. 3*c*, where a tubule can be represented by an index (m, n). This tubule can be realized by rolling up a sheet of hexagons so as to superimpose the origin (0, 0) on the hexagon (m, n). A tubule $(m, -n)$ is chiral with the opposite handedness to (m, n), and thus they should be optically active, but they cannot be distinguished by the diffraction experiment. The tubules which were observed frequently on the histogram (Fig. 2) have values of (m, n) in the hatched areas. On the electron diffraction pattern in Fig. 3*a*, α and D are measured as 7° and 1.37 nm, respectively. This tube can be indexed as (18, 2) or its enantiomer (18, −2), and should behave as a semiconductor according to electronic band structure calculations[6,16]. We should mention here that α, or helicity, varies for a given tubule diameter.

We speculate that the single-shell tubules might be the embryo for the multi-shell tubules. In our proposed model for the nanotube growth[17,18], the tubule ends are open so that carbon atoms are easily captured at dangling bonds, and the multi-shell tubules grow in the direction of the tube axis and also perpendicular to it. The latter growth is associated with layer-by-layer growth on the tubule surface. In the single-shell tubes, we assume that axial growth dominates over layer growth. We speculate that the iron in the present experiments acts as a homogeneous catalyst in the vapour phase. □

Received 23 April; accepted 1 June 1993.

1. Iijima, S. *Nature* **354**, 56–58 (1991).
2. Ajayan, P. M. & Iijima, S. *Nature* **361**, 333–334 (1993).
3. Ajayan, P. M. *et al. Nature* **362**, 522–523 (1993).
4. Tsang, S.C., Harris, P.J. F. & Green, M.L. *Nature* **362**, 520–522 (1993).
5. Pederson, M. R. & Broughton, J. O. *Phys. Rev. Lett.*, **69**, 2687–2692 (1992).
6. Hamada, N., Sawada, S. & Oshiyama, S. *Phys. Rev. Lett.* **68**, 1579–1581 (1992).
7. Mintmire, J. W., Dunlap, B. I. & White, C. T. *Phys. Rev. Lett.* **68**, 631–634 (1992).
8. Saito, R., Fujita, F., Dresselhaus, G. & Dresselhaus, M. S. *Phys. Rev.* B **46**, 1804–1811 (1992).
9. Robertson, D. H., Brenner, D. W. & Mintmire, J. W. *Phys. Rev.* B **45**, 12592–12595 (1992).
10. Ebbesen, T.W. & Ajayan, P.M. *Nature* **368**, 220–222 (1992).
11. Ando, Y. & Iijima, S. *Jpn. J. appl. Phys.* **32**, L107–L109 (1993).
12. Oberlin, A. & Endo, M. *J. Cryst. Growth* **32**, 335–349 (1976).
13. Iijima, S. *Chem. Scripta* **14**, 117–123 (1978-79).
14. Iijima, S., Ichihashi, T. & Ando, Y. *Nature* **356**, 776–778 (1992).
15. Ajayan, P.M. Ichihashi, T. & Iijima, S. *Chem. Phys. Lett.* **202**, 384–388 (1992).
16. White, C. T., Robertson, D. H. & Mintmire, J. W. *Phys. Rev.* B **47**, 5485–5488 (1993).
17. Iijima, S., Ajayan, P. M. & Ichihashi, T. *Phys. Rev. Lett.* **69**, 3100–3103 (1992).
18. Iijima, S. *Mat. Sci. Enging* B. (in the press).

Cobalt-catalysed growth of carbon nanotubes with single-atomic-layer walls

D. S. Bethune, C.H. Klang*, M. S. de Vries, G. Gorman, R. Savoy, J. Vazquez & R. Beyers

IBM Research Division, Almaden Research Center, 650 Harry Road, San Jose, California 95120-6099, USA

CARBON exhibits a unique ability to form a wide range of structures. In an inert atmosphere it condenses to form hollow, spheroidal fullerenes[1–4]. Carbon deposited on the hot tip of the cathode of the arc-discharge apparatus used for bulk fullerene synthesis will form nested graphitic tubes and polyhedral particles[5–8]. Electron irradiation of these nanotubes and polyhedra transforms them into nearly spherical carbon 'onions'[9]. We now report that covaporizing carbon and cobalt in an arc generator leads to the formation of carbon nanotubes which all have very small diameters (about 1.2 nm) and walls only a single atomic layer thick. The tubes form a web-like deposit woven through the fullerene-containing soot, giving it a rubbery texture. The uniformity and single-layer structure of these nanotubes should make it possible to test their properties against theoretical predictions[10–13].

The initial aim of our experiments was to produce metallofullerenes and graphite-encapsulated nanocrystals of magnetic atoms. Electrodes were prepared by boring 4-mm-diameter holes in 6-mm-diameter graphite rods and filling them with mixtures of pure powdered metals (Fe, Ni or Co) and graphite. These filled anodes (~ 2 at % metal) were vaporized with a current of 95–105 A in 100–500 torr of He in our arc fullerene generator. The results obtained with cobalt were unique.

When a Co-containing rod was used, what looked like spider webs formed in the chamber, draping between surfaces. The soot on the chamber walls was rubbery and could be peeled off in long strips. Normal fullerene soots (and those made with Fe- or Ni-containing rods) are crumbly. The soot and the web material were ferromagnetic. A transmission electron microscope (TEM) image of the web material (Fig. 1) shows that the web consists of rounded soot particles a few tens of nanometres across, linked together by fine fibres. Individual threads can be traced for several micrometres. In some cases several fibres converge on a soot particle. Embedded within the soot particles are round cobalt clusters with diameters ranging from a few nanometres to roughly 20 nm. Both electron and X-ray diffrac-

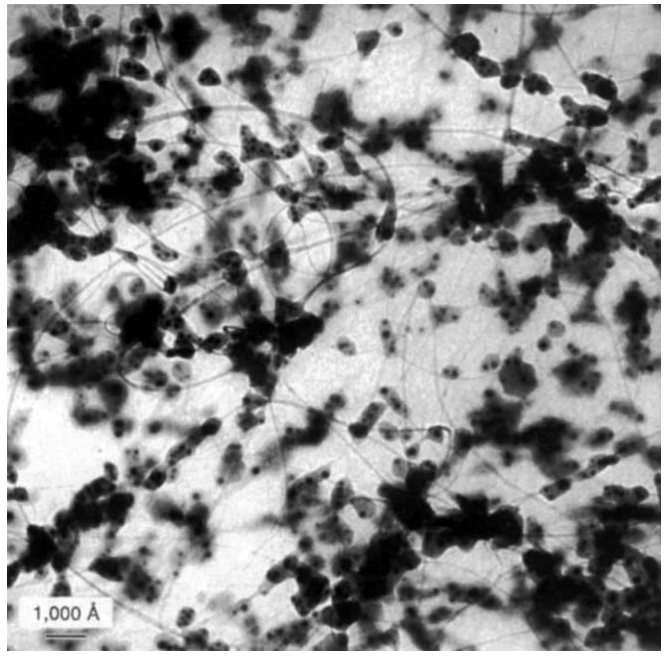

FIG. 1 Transmission electron micrograph of web-like material showing strands of thread-like fibres and cobalt clusters (dark spots) embedded in carbon soot particles. This image and those in Figs 2 and 3 were obtained using a Topcon 002B microscope operating at 200 kV and a Gatan Model 679 slow-scan camera to acquire digital images, which can then have the contrast enhanced to reveal the nanotubes.

*Affiliated with the Materials and Molecular Simulation Center, Beckman Institute, California Institute of Technology, Pasadena, California 91125, USA.

tion patterns showed that these clusters are face-centred-cubic Co. This indicates that the clusters were rapidly quenched, as Co is normally hexagonal-close-packed below 400 °C.

Scanning electron microscope (SEM) images show that the rubber soot deposits from the chamber walls contain thin fibres and soot particles similar to those in the web material, but with the particles in greater relative abundance. The carbon around the cobalt clusters consists partly of fullerenes, which can be extracted from the soot in typical amounts using toluene. Laser-desorption/laser-ionization mass-spectrometry of the raw soot showed a CoC_{60} peak, but this species was not found in a toluene extract of the soot.

A higher-magnification TEM image (Fig. 2) reveals the structures underlying the fibre and web formation. Carbon nanotubes with single-atomic-layer walls and diameters of 1.2 ±0.1nm are ubiquitous. The tubules apparently crossed, aggregated and tangled before being encased. Although the tubules are mostly coated with non-graphitic carbon, bare sections are also evident. Figure 3 (at still higher magnification) shows a bare nanotube with several round objects, comparable in size to fullerenes with 60–100 carbons, adhering to it. The circumference of the nanotubes would correspond to a belt of 15 or 16 edge-sharing hexagons with 0.142-nm sides.

Carbon fibres grow under diverse conditions[14–16]. Graphitic whiskers 1–5 μm in diameter and centimetres in length can be grown on the extremely hot cathode of a carbon arc run in high-pressure argon[17]. Under similar conditions (but at lower pressures), tubular graphitic structures with 2–30 nm diameters and micrometre lengths form in the cathode deposits in an arc-fullerene generator[5–7]. These nanotubes typically have walls 2–50 atomic layers thick. On the other hand, in the presence of transition-metal catalyst particles, vapour-grown carbon fibre can be produced by pyrolysing a hydrocarbon/carrier-gas mixture at temperatures between 500 °C and 1,200 °C (refs 14–16). Yacaman *et al.*[18] recently reported that some fibres produced by this method resemble the hollow graphitic tubes seen in fullerene-generator cathode deposits.

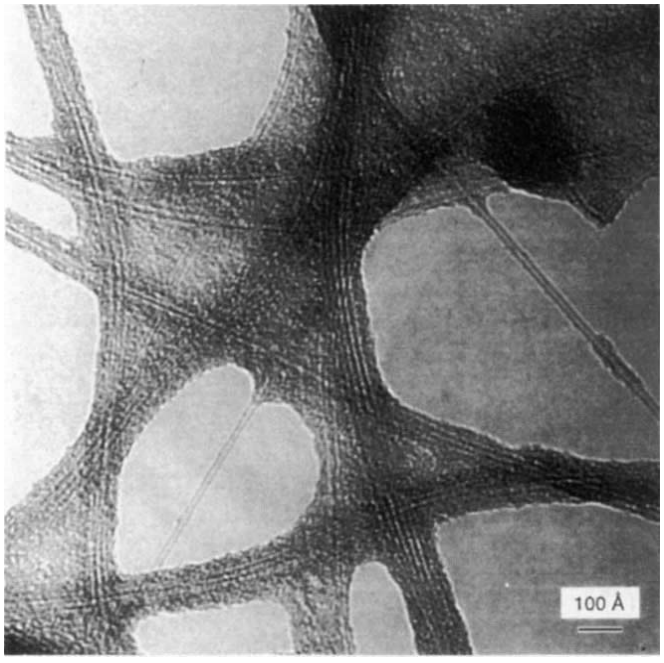

FIG. 2 TEM image at higher magnification showing details of the web-like material. Running through the deposited non-graphitic carbon are single-walled nanotubes about 1.2 nm in diameter. Bare portions of these nanotubes are also evident. The dark spot in the upper-right corner is a cobalt cluster.

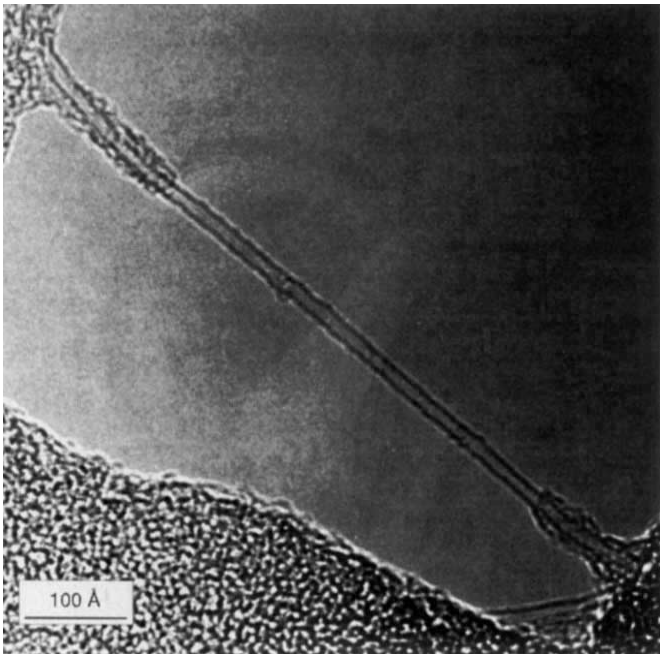

FIG. 3 TEM image of a bare section of a single-walled nanotube. The round objects adhering to the tube have diameters corresponding to fullerenes with 60–100 carbons.

In contrast to these multilayered fibres and tubes, our cobalt-catalysed nanotubes have single-atomic-layer walls and a common diameter (~ 1.2 nm). They grow from carbon vapour (with no dissociation of hydrocarbon needed) at helium pressures in the range 100–500 torr. Fullerenes form abundantly at the same time. Under the conditions we used, no fibre growth was observed using Fe, Ni or a 50:50 Ni:Cu mixture, all of which catalyse fibre growth in the presence of hot gaseous hydrocarbons[19,20]. We believe, therefore, that cobalt plays a special role in catalysing the formation of these single-walled tubules, and suggest that a specific nucleation process may be responsible for their highly uniform diameter. For the moment the relationship between the nanotubes and the cobalt clusters is obscured by the encasing layer of carbon. The nanotubes are found in relatively cold regions of the chamber, co-condensed with (and mostly coated by) fullerene soot. It may be possible to control the amount of carbon that forms on the nanotubes by modifying the growth conditions, and the crystallinity of this carbon by post-annealing the coated nanotubes at high temperature. Such measures have been used to modify vapour-grown carbon fibres[14], and could be important in attempting to exploit the uniformity of these vapour-grown nanotubes to develop new types of carbon fibres.

It may also be possible to isolate bulk quantities of bare, single-walled nanotubes. Such structures constitute a new type of all-carbon polymer. Theoretical calculations predict that they can be metallic or semiconducting, depending on their helical pitch[10,11]. They might draw species into their interiors by capillary action, and they may be useful as catalytic containers, nanowires and solenoids[21]. The recent success of Ajayan *et al.*[22] in filling nanotubes with lead supports some of these ideas. The availability of the single-walled carbon nanotubes reported here should permit characterization and further experiments. □

Received 24 May; accepted 3 June 1993.

1. Kroto, H. W., Heath, J. R., O'Brien, S. C., Curl, R. F. & Smalley, R. E. *Nature* **318**, 162–163 (1985).
2. Krätschmer, W., Fostiropoulos, K. & Huffman, D. R. *Chem. Phys. Lett.* **170**, 167–170 (1990).

3. Krätschmer, W., Lamb, L. D., Fostiropoulos, K. & Huffman, D. R. *Nature* **347**, 354–358 (1990).
4. Meijer, G. & Bethune, D. S. *J. chem. Phys.* **93**, 7800–7802 (1990).
5. Iijima, S. *Nature* **354**, 56–58 (1991).
6. Iijima, S., Ichihashi, T. & Ando, Y. *Nature* **356**, 776–778 (1992).
7. Ebbesen, T. W. & Ajayan, P. M. *Nature* **358**, 220–222 (1992).
8. Saito, Y., Yoshikawa, T., Inagaki, M., Tomita, M. & Hayashi, T. *Chem. Phys. Lett.* **204**, 277–282 (1993).
9. Ugarte, D. *Nature* **359**, 707–708 (1992).
10. Hamada, N., Sawada, S. & Oshiyama, A. *Phys. Rev. Lett.* **68**, 1579–1581 (1992).
11. Mintmire, J. W., Dunlap, B. I. & White, C. T. *Phys. Rev. Lett.* **68**, 631–634 (1992).
12. Saito, R., Fujita, M., Dresselhaus, G. & Dresselhaus, M. S. *Phys. Rev.* B**46**, 1804–1811 (1992).
13. Robertson, D. H., Brenner, D. W. & Mintmire, J. W. *Phys. Rev.* B**45**, 12592–12595 (1992).
14. Endo, M. *Chemtech* **18**, 568–576 (1998).
15. Baker, R. T. *Carbon* **27**, 315–323 (1989).
16. Tibbetts, G. G. *J. Cryst. Growth* **73**, 431–438 (1985).
17. Bacon, R. *J. appl. Phys.* **31**, 283–290 (1960).
18. Jose-Yacaman, M., Miki-Yoshida, M., Rendon, L. & Santiesteban, J. G. *Appl. Phys. Lett.* **62**, 657–659 (1993).
19. Baker, R. T. & Harris, P. S. in *Chemistry and Physics of Carbon*, Vol. 14, 83–165 (Marcel Dekker, New York, 1978).
20. Kim, M. S., Rodriguez, N. M. & Baker, R. T. *J. Catal.* **131**, 60–73 (1991).
21. Pederson, M. R. & Broughton, J. Q. *Phys. Rev. Lett.* **69**, 2689–2692 (1992).
22. Ajayan, P. M. & Iijima, S. *Nature* **361**, 333–334 (1993).

ACKNOWLEDGEMENTS. We thank W. A. Goddard III, R. D. Johnson, C. S. Yannoni, C. T. Rettner and J. R. Salem for discussions. C. H. K. acknowledges partial support by the NSF and the Materials and Molecular Simulation Center (supported by DOE-AICD, Allied-Signal, BP America, Asahi Chemical, Asahi Glass, Chevron, B. F. Goodrich and Xerox).

Synchronous changes in seawater strontium isotope composition and global climate

Steven C. Clemens, John W. Farrell* & L. Peter Gromet

Geological Sciences, Brown University, Providence, Rhode Island, 02912-1846, USA

THE $^{87}Sr/^{86}Sr$ ratio of sea water has increased gradually over the past 40 Myr, suggesting a concomitant increase in global chemical weathering rates[1–6]. Recently, Dia *et al.*[7] analysed a 250-kyr $^{87}Sr/^{86}Sr$ record, and found superimposed on this gradual increase higher-frequency $^{87}Sr/^{86}Sr$ variations which appeared to follow a 100-kyr cycle; this periodicity corresponds to one of the prominent cycles in the Earth's orbital parameters, which are known to modulate the patterns of solar insolation and hence climate[8–10]. The resolution of this record was, however, insufficient to establish the phase relationship between the $^{87}Sr/^{86}Sr$ variations and global climate cycles. Here we present a high-resolution seawater $^{87}Sr/^{86}Sr$ record spanning the past 450 kyr. We find that maxima and minima in $^{87}Sr/^{86}Sr$ coincide with minima and maxima, respectively, in continental ice volume (from the SPECMAP oxygen isotope record[20]), apparently suggesting that there was less chemical weathering in arid glacial periods than in the more humid interglacials. During glacial–interglacial transitions, however, seawater $^{87}Sr/^{86}Sr$ changes at a rate of ~ 1 p.p.m. kyr^{-1}, approximately three times that evaluated by Dia *et al.*[7]. Mass-balance calculations illustrate that simple changes in modern chemical weathering regimes cannot fully account for such rapid changes, suggesting that we need to revise current ideas about strontium reservoirs and the mechanisms for exchange between them.

To evaluate fine structure in the past 450 kyr of the seawater $^{87}Sr/^{86}Sr$ record, we measured the $^{87}Sr/^{86}Sr$ ratios in 77 samples of marine carbonate (planktonic foraminifera) from Ocean Drilling Program/site 758 in the equatorial Indian Ocean (Fig 1, Table 1). This record can be interpreted as a global ocean signal provided that (1) seawater $^{87}Sr/^{86}Sr$ is globally homogeneous within the mixing time of the ocean, (2) biogenic calcite is precipitated in equilibrium with seawater $^{87}Sr/^{86}Sr$, and (3) the $^{87}Sr/^{86}Sr$ signal measured in planktonic foraminifera is derived from Sr in the calcite lattice and not associated phases such as fine clays or diagenetic precipitates adhering to the skeletal calcite. Results from several studies suggest that these conditions are met. Measurements of seawater $^{87}Sr/^{86}Sr$ from Pacific and Atlantic surface and deep waters demonstrate the homogeneity of $^{87}Sr/^{86}Sr$ in the modern global ocean to within 6 p.p.m., well within the analytical error of measurement[11]; the $^{87}Sr/^{86}Sr$ of biogenic calcite from globally distributed planktonic foraminifera and bivalves is indistinguishable from modern sea water [3,7,11,12]; the $^{87}Sr/^{86}Sr$ of calcite from planktonic and benthic foraminifera is indistinguishable, indicating equilibrium precipitation in surface as well as deep waters[13].

To minimize the contribution of Sr from noncarbonate material, foraminifera were prepared for $^{87}Sr/^{86}Sr$ measurement as in previous studies[2,14,15], by sonification in ultrapure water followed by dissolution of the calcite in weak acetic acid. To investigate further the possibility of contamination by noncarbonate phases, we cleaned a subset of our samples following more rigorous procedures[16,17] designed to remove fine clays, oxidize organic matter and reduce precipitated metal oxides before dissolving the calcite lattice. All but one of the paired samples (N=17) yielded analytically indistinguishable results (Table 1).

Another approach to testing the validity of the site 758 $^{87}Sr/^{86}Sr$ record as a global signal is duplication of the results in other oceans with different sedimentary environments, using different foraminifera species. Comparison with a lower resolution record from the Pacific[7] shows strong similarities and some differences (Fig. 1). As with the the well documented ice-age cyclicity in $\delta^{18}O$ (refs 18–21), both $^{87}Sr/^{86}Sr$ records show 100-kyr fluctuations with higher values during interglacial stages and lower values during glacial stages indicating that, to first order, both sites record a global ocean signal. However, the site 758 record indicates that glacial–interglacial transitions in $^{87}Sr/^{86}Sr$ occur more or less simultaneously with changes in ice volume ($\delta^{18}O$), whereas $^{87}Sr/^{86}Sr$ in the V28-238 record appears to lead the global ice-volume signal by 10–15 kyr at deglaciations. Similarly, relative amplitude differences between the two strontium records exist within oxygen isotope stages 3 and 6. One possible explanation of these differences is that the

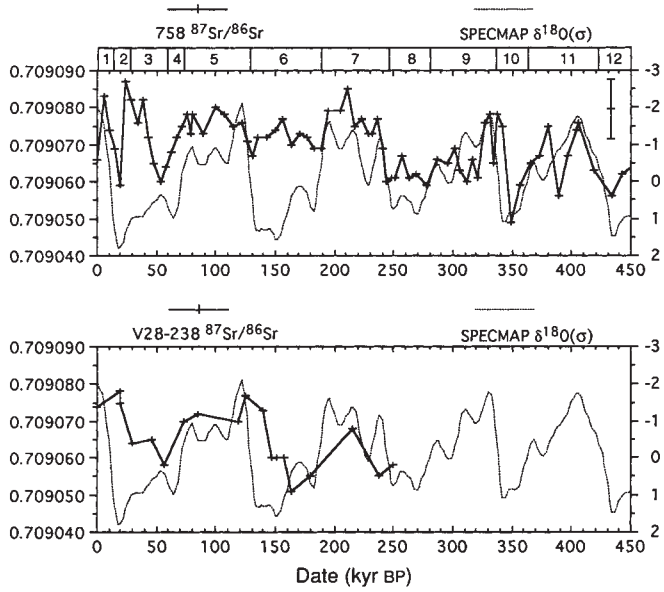

FIG. 1 Seawater $^{87}Sr/^{86}Sr$ records compared to the SPECMAP stacked $\delta^{18}O$ record[20] of global ice-volume. Indian Ocean site 758 (top) (error bar represents $\pm 1\sigma$) and Pacific Ocean V28-238 (bottom; ref. 7). Both records are plotted relative to an NBS-987 value of 0.710150. Oxygen isotopic stages[20] are labelled at the top (even numbers represent glacial intervals).

* Present address: University of Bristish Columbia, Vancouver, British Columbia, V6T1Z4.